Importance of Electronegativity Differences and Surface Structure in Molecular Dissociation Reactions at Transition Metal Surfaces

Paul Crawford and P. Hu*

School of Chemistry and Chemical Engineering, The Queen's University of Belfast, Belfast, BT9 5AG, U.K.

Received: June 5, 2006; In Final Form: September 16, 2006

The dissociative adsorption of N_2 has been studied at both monatomic steps and flat regions on the surfaces of the 4d transition metals from Zr to Pd. Using density functional theory (DFT) calculations, we have determined and analyzed the trends in both straight reactivity and structure sensitivity across the periodic table. With regards to reactivity, we find that the trend in activation energy (E_a) is determined mainly by a charge transfer from the surface metal atoms to the N atoms during transition state formation, namely, the degree of ionicity of the N-surface bond at the transition state. Indeed, we find that the strength of the metal−N bond at the transition state (and therefore the trend in E_a) can be predicted by the difference in Mulliken electronegativity between the metal and N. Structure sensitivity is analyzed in terms of geometric and electronic effects. We find that the lowering of E_a due to steps is more pronounced on the right-hand side of the periodic table. It is found that for the early transition metals the geometric and electronic effects work in opposition when going from terrace to step active site. In the case of the late 4d metals, however, these effects work in combination, producing a more marked reduction in E_a.

Introduction

It has long been realized that insight into heterogeneous catalytic processes may be gained by studying chemical reactions occurring on surfaces.[1−3] Of particular importance is the dissociative adsorption of diatomic molecules over transition metal surfaces. There are two reasons for this: (i) These reaction steps commonly provide important intermediates; the production of which is often rate limiting in catalytic mechanisms. For example, in ammonia synthesis,[4−13] N_2 dissociates, providing the surface with atomic N, which is subsequently hydrogenated to NH_3. Furthermore, both Fischer−Tropsch synthesis[14−20] and NO reduction in car exhausts begin with the dissociation of CO and NO, respectively. (ii) Transition metal particles are the active component of many real catalysts.

Both theoretical and empirical models have been employed to explain how the dissociative ability of one transition metal varies from the next. Reactivity has been successfully correlated to simple properties of the metal surface such as the local density of one electron states at the Fermi level[21−23] and the number of holes in the d-bands.[24] In addition, Hammer and Norskov have formulated a quantitative reactivity measure based on the d-band center model.[25] Moreover, dissociative processes over transition metals have been shown to follow Bronsted−Evans−Polanyi (BEP) relationships.[26−27] That is, the activation energies are observed to correlate with the reaction enthalpies. This relationship has found a number of applications in the field of heterogeneous catalysis.[28−30]

Another important aspect of molecular dissociation over transition metal surfaces is structure sensitivity. That is, the reaction rates of some surface processes are seen to increase with increasing surface defects. Structure sensitivity is determined by two aspects of the surface active site: (i) the geometric arrangement of the surface atoms at the active site (the geometric effect) and (ii) how the bonding ability of the active site atoms varies with their coordination environment (electronic effect). Hammer et al. considered the electronic effect by studying the chemisorption of CO on different Pt surfaces.[31] Using the d-hybridization model, it was determined that the variation in bond strength mainly arose from $2\pi^*$−d coupling; the stronger this coupling, the stronger the CO−metal bonding. It was found that as the d-band center shifted toward the Fermi level the $2\pi^*$−d coupling increased.[31] Indeed, density functional theory (DFT) calculations showed that CO chemisorption energy varied linearly with d-band center height, which shifted toward the Fermi level with decreasing coordination of the surface metal atoms considered.

Liu and Hu studied the structure sensitivity of CO dissociation on Rh and Pd.[32] They found that the activation energy was significantly reduced on step defects relative to terraces. It was concluded that the more favorable five atom arrangement of the step site, compared to the four atom active site on terraces, was more important in reducing the barrier than the local electronic effect of the uncoordinated step edge atoms, i.e., the geometric effect was the important factor in the case of CO dissociation. Dahl et al., using adsorption experiments and DFT calculations, showed that N_2 dissociation on Ru(001) is completely dominated by steps[33] and that the difference in activation energy between the terrace and step is around 1.5 eV. DFT calculations by Hammer show that the activation energy for NO dissociation on Ru is also around 1.5 eV lower at step sites.[34] In this case, the greater bonding ability of the step edge atoms was found to account for the lower activation energy at steps.

The above theoretical and empirical studies have provided a great deal of insight into the chemistry of molecular dissociation over transition metal surfaces. However, there is still a call for theoretical reactivity studies of step edges, to determine when and why they are of importance in the modeling of catalytic reactions. Furthermore, to date, there has been little done to

* Corresponding author: p.hu@qub.ac.uk.

10.1021/jp063472u CCC: $33.50
Published on Web 11/18/2006

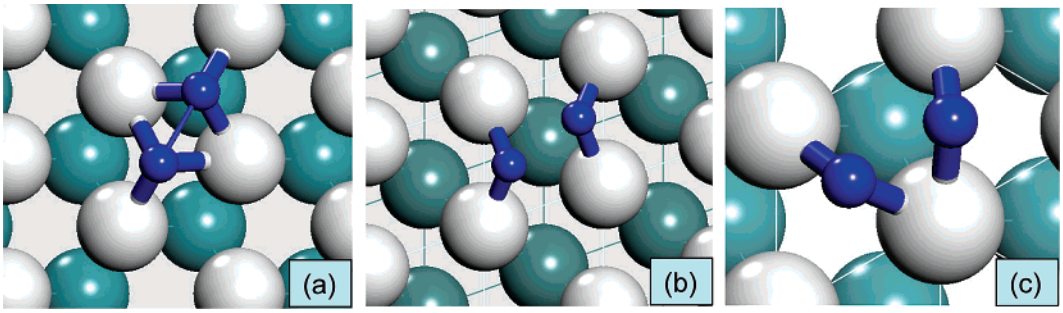

Figure 1. Energetically most stable transition state geometry types for the dissociation of N_2 over the close-packed surfaces of the FCC and HCP metals and the more open (110) surfaces of the BCC metals. (a) Double-hollow site transition states determined for the close-packed surfaces of the HCP and FCC metals. (b) Double-bridge site transition states determined over the 110 surfaces of the BCC metals. (c) Double-bridge site transition states observed over the close-packed surfaces of the FCC and HCP metals.

TABLE 1: Main Geometrical Parameters of Our Calculated Transition State Geometries on Each of the Metal Surfaces[a]

surface	transition state type	$d(N^{fcc}-M)$ ($d(N^{br}-M)$) Å	$d(N^{hcp}-M)$ ($d(N^{br}-M)$) Å	$d(N-N)$ Å	E_a (eV)	Σq^{TS} (electrons)
Zr(001)	hollow site	2.102	2.129	1.830	−2.47	−1.29
Nb(110)	bridge site	1.955	1.955	1.895	−1.86	−1.12
Mo(110)	bridge site	1.962	1.962	1.839	−1.25	−1.00
Tc(001)	hollow site	2.059	2.003	1.638	−0.74	−0.94
Ru(001)	hollow site	2.072	1.985	1.685	1.17	−0.87
Rh(111)	hollow site	2.049	1.990	1.849	1.95	−0.78
Pd(111)	bridge site	1.945	1.947	2.012	3.15	−0.53

[a] The first data column refers to the average metal−N distance at the fcc hollow site (or bridge site), and the second refers to the average metal−N distance at the hcp hollow site (or bridge site). The activation energies (E_a) correspond to the lowest energy reaction pathways for the dissociative adsorption of N_2 over the flat surfaces of the 4d metals from Zr to Pd. The sum of the atomic charges on the N atoms at the transition state (Σq^{TS}), as determined by Mulliken population analysis, are also given.

examine the usefulness of reactivity descriptors, such as those of the hard-soft-acid-base (HSAB) theory of molecular chemistry,[35−38] in the context of transition metal surface chemistry. In the present work, we address both the issues of direct reactivity and structure sensitivity by studying the dissociative adsorption of N_2 over the 4d transition metals from Zr to Pd at both monatomic steps and flat regions. This paper is organized as follows: in section 1, we focus on straight reactivity by dealing with the trend in activation energies on the flat surfaces, and in section 2, we address the issue of structure sensitivity and how it changes across the periodic table by comparing reactivity at monatomic steps and flat regions on each metal surface.

Calculation Details

The DFT calculations were performed using the castep code.[39] Ultrasoft pseudopotentials were used to describe the ionic cores. The wave functions were expanded in a plane wave basis set up to a kinetic energy of 360 eV. The effects of exchange and correlation were described within generalized gradient approximation (GGA); the PBE exchange-correlation functional[40] was used in all of the calculations. Monkhorst−Pack *k*-point sampling was utilized throughout. Spin polarized calculations were performed in the case of Fe, Co, and Ni. Both stepped and flat surfaces were modeled as a periodic array of slabs. The slabs consisted of effectively 3 layers of metals atoms fixed at their bulk truncated positions. A vacuum spacing of approximately 10 Å was left between the slabs. In all of the models, calculated lattice constants are used. A p(2 × 2) unit cell was used for the flat surfaces, with 3 × 3 × 1 *k*-point sampling.

Monatomic steps were generated for the HCP metals by removing 2 rows of atoms from a (001) surface. A p(2 × 5) unit cell was used for the HCP stepped surfaces with 3 × 2 × 1 *k*-point sampling. In the case of the BCC and FCC metals, steps were generated by cleaving a (210) and (211) surface, respectively. For the stepped surfaces of both crystal types, a p(2 × 1) unit cell with 3 × 3 × 1 *k*-point sampling was used. The transition states were identified using the constrained-minimization technique, which constrains the distance between the reacting atoms, while optimizing the remaining degrees of freedom. Transition states were identified when (i) the forces on the atoms were zero and (ii) the energy was a maximum along the reaction coordinate, but a minimum with respect to all the remaining degrees of freedom. Previous work has shown that the above setting provides sufficient accuracy.[32,41−43]

1. Reactivity

1.1. Results. We will first examine the trend in reactivity for N_2 dissociative adsorption on the most stable flat surfaces of the 4d transition metals, i.e., (111) surfaces for FCC metals, (001) surfaces for HCP metals, and (110) surfaces for BCC metals. Extensive calculations were performed in order to determine the lowest energy transition states on each surface. The activation energy in all of the following discussions is taken as the difference in total energy between the molecule−surface transition state complex and N_2 in the gas phase plus a clean surface

$$E_a = E(\text{surface}/N_2^*) - \{E(N_2)_g + E(\text{surface})\} \qquad (1)$$

where $E(\text{surface}/N_2^*)$, $E(N_2)_g$, and $E(\text{surface})$ are the total energies of the N_2/surface transition state complex, the N_2 molecule in the gas phase, and the clean metal surface, respectively.

From Table 1, it can be seen that the lowest energy reaction pathway changes on moving across the period from Zr to Pd. On Zr(001), a double-hollow site transition state is observed to provide the lowest energy reaction pathway. On Nb(110) and Mo(110), double-bridge site transition states are observed to be the most stable. In the case of Ru(001) and Rh(111), double-

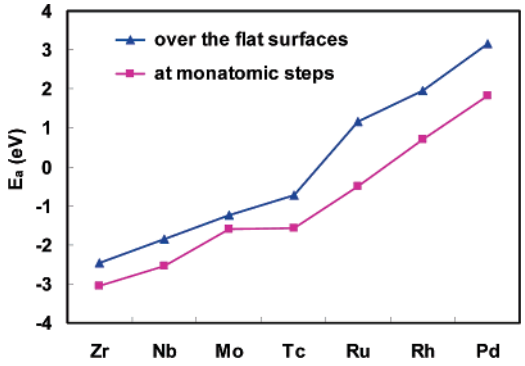

Figure 2. Activation energies that correspond to the lowest energy reaction pathways for the dissociative adsorption of N_2 over the flat surfaces of the 4d transition metals from Zr to Pd (upper curve) and activation energies that correspond to the lowest energy reaction pathways for the dissociative adsorption of N_2 at monatomic steps on the surfaces of the 4d metals from Zr to Pd (lower curve).

hollow site transition states are the most energetically favorable. Interestingly, on Pd(111), a double-bridge site transition state geometry is found to be the most stable (Figure 1). Figure 2 shows a plot of the activation energies corresponding to the lowest energy reaction pathways for the dissociative adsorption of N_2 over the flat surfaces of the 4d transition metals from Zr to Pd. As can be seen, E_a increases on moving from left to right across the period. It is noticed that there is a large jump in E_a on moving from Tc to Ru and that an actual reaction barrier only exists from Ru onward, on moving from left to right across the period.

1.2. Analysis and Discussion. In the following discussions, we first address the trend in reactivity (Figure 2) in terms of geometric and electronic effects; that is to say, how the intrinsic electronic nature of the metal and the geometry of the surface active site affect the magnitude of E_a. To differentiate these effects, we have separated the activation energy into two parts: (i) The total chemisorption energy at the transition state (ΣE_{chem}(N*). This sum represents the chemisorption energy of N atom A at its transition state position, but in the absence of N atom B, plus the chemisorption energy of N atom B at its transition state position, but in the absence of N atom A. This term therefore represents the bonding potential of the surface active site while neglecting the interaction energy between the two N atoms, i.e., it gives a measure of the electronic effect. (ii) The interaction energy between the N atoms at the transition state (E_{int}). This term depends on the geometry of the surface active site and can therefore be considered to be a secondary electronic effect or a geometric effect. The activation energy is therefore decomposed as

$$E_a = \sum E_{chem}(N^*) + E_{\{int\}} + D(N_2) \qquad (2)$$

where the first two terms in eq 2 have been described above and $D(N_2)$ is the bond dissociation energy of N_2 in the gas phase (calculated in this work as 9.587 eV). This decomposition has been used by a number of groups to study dissociative adsorption on transition metal surfaces and is quite standard.[32,34] The activation energies for the dissociative adsorption of N_2 over the flat 4d transition metal surfaces have been decomposed in the above manner, and values from this analysis are given in Table 2.

This data reveals a number of interesting trends. It is observed that the interaction energy is seen to be relatively small in comparison with ΣE_{chem}(N*). There is also much greater variation in ΣE_{chem}(N*) than E_{int} on moving across the period. More importantly, the analysis shows that the trend in E_a follows

TABLE 2: Calculated Values Corresponding to the Activation Energy Decomposition Scheme Discussed Above (Equation 2)[a]

surface	TS type	ΣE_{chem}(N*) (eV)	E_{int} (eV)
Zr(001)	hollow	−14.841	2.784
Nb(110)	bridge	−12.868	1.422
Mo(110)	bridge	−12.373	1.530
Tc(001)	hollow	−12.492	2.167
Ru(001)	hollow	−10.190	1.776
Rh(111)	hollow	−8.996	1.355
Pd(111)	bridge	−7.205	0.766

[a] ΣE_{chem}(N*) is the sum of the chemisorption energy of both N atoms at their respective transition state locations, and E_{int} is the interaction energy between the N atoms at the transition state.

TABLE 3: E_{chem}(N), the Chemisorption of Atomic N at its Equilibrium Bonding Site on a Selection of 3d, 4d, and 5d Flat Transition Metal Surfaces[a]

metal surface	equil bonding site	ΔX (eV)	E_{chem}(N) (eV)	atomic charge (electrons)
Ti(001)	fcc	3.844	−7.844	
V(110)	3-fold hollow	3.664	−7.124	
Fe(110)	3-fold hollow	3.274	−6.205	
Co(001)	hcp	3.034	−4.927	
Ni(111)	hcp	2.904	−4.951	
Cu(111)	fcc	2.814	−3.805	
Zr(001)	fcc	3.774	−7.654	−0.78
Nb(110)	3-fold hollow	3.474	−6.882	−0.72
Mo(110)	3-fold hollow	3.384	−6.827	−0.65
Tc(001)	hcp	3.394	−6.688	−0.56
Ru(001)	hcp	3.094	−5.556	−0.53
Rh(111)	hcp	3.004	−4.847	−0.45
Pd(111)	fcc	2.854	−4.367	−0.28
Hf(001)	fcc	3.879	−7.205	
Ta(110)	3-fold hollow	3.200	−7.051	
W(110)	3-fold hollow	2.906	−6.041	
Re(001)	hcp	3.291	−6.597	
Os(001)	hcp	2.401	−5.451	
Ir(111)	hcp	1.961	−5.033	
Pt(111)	fcc	1.732	−4.464	

[a] ΔX is the difference in metal−N electronegativity estimated using Mulliken's definition and atomic ionization energies and electron affinities. Also given is the atomic charge on N, as determined by Mulliken charge analysis, for the 4d metals from Zr to Pd.

closely that of ΣE_{chem}(N*) (the correlation coefficient R^2 is observed to be 0.97). We should mention at this point that ΣE_{chem}(N*) is found to be almost identical to 2 times the chemisorption of N (E_{chem}(N)) at its equilibrium chemisorption site on the above surfaces. Namely, due to the large internuclear separation between the N atoms at the transition state, they interact with the surface as if they were individual atomic species. Indeed, the correlation between ΣE_{chem}(N*) and $2 \times E_{chem}$(N) is quantitative with $R^2 = 0.99$ (Table 3). This however prompts a fundamental question: can we estimate, without first principle calculations, the trend in chemisorption energy of atomic N across the transition series? If we could, the relative activity of a particular metal toward N_2 dissociation could be estimated.

Schwegmann et al. explained the chemisorption of N on Ru(001) using a simple two-level tight binding model.[44] They determined that the strength of the bond was due to two main effects: (i) A bonding hybrid orbital is formed, consisting mainly of the sp hybrid orbitals of N and the d_z^2-like orbitals of the three nearest neighbor Ru atoms. This results in an increase in the charge density at the N atom. (ii) The antibonding states are pushed above the Fermi-level and hence do not weaken the bond. DFT calculations by Cao et al. showed that N atoms adsorbed on Ru clusters carry a significant negative

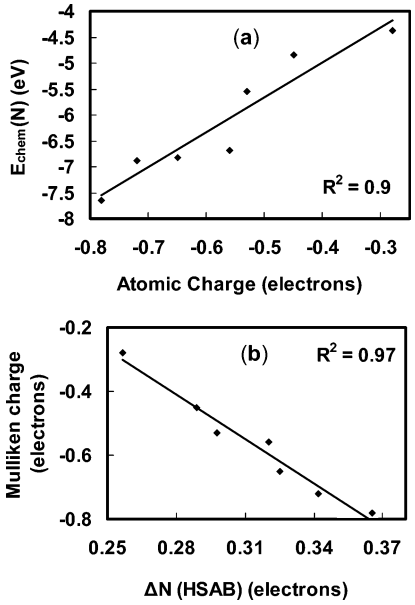

Figure 3. (a) Correlation between the atomic charge on the chemisorbed N atom, as determined by Mulliken charge analysis, and the strength of metal−N bonding. (b) Agreement between the amount of charge transferred (ΔN) as predicted by eq 3 and the actual atomic charge on the chemisorbed N atom, as determined by Mulliken charge analysis.

charge.[45] They further suggest that the activation of N_2 on transition metal clusters is controlled by charge transfer from the metal atoms to the $2\pi^*$ orbital of N_2. Charge transfer is therefore seen to play an important part in how N interacts with transition metals. Rodriquez and Goodman studied the bonding of transition metal adatoms on dissimilar transition metal surfaces using thermal desorption mass spectroscopy, UV photoelectron spectroscopy, and X-ray photoelectron spectroscopy. They found that the substrate−adatom bond strength was proportional to the charge transferred between them.[46] That is to say, bond strength was found to be proportional to the degree of ionicity of the adatom− substrate bond.

To test the applicability of the above ideas to the adsorption of atomic N on transition metal surfaces, we have calculated the Mulliken charge on N adsorbed at its equilibrium position on the flat surfaces of the 4d transition metals from Zr to Pd. Although the absolute magnitude of such atomic charges has little physical significance, due to basis set sensitivity, their relative magnitude has been successfully applied to determine ionicity in bulk materials.[47] The chemisorption energies of atomic N and the respective Mulliken charges are given in Table 3, and the relationship between chemisorption energy and Mulliken charge is shown in Figure 3a. As can be seen there is good agreement between the amounts of charge transferred to the N atom and the strength of the metal−N bonding. That is, bond strength is seen to relate to the degree of ionicity of the bond. What is more, we have found that the variation in the amount of charge transferred to the N atom across the period can be nicely predicted by the charge-transfer expression from the HSAB theory of molecular chemistry[48]

$$\Delta N = \frac{(\mu_M - \mu_N)}{(\eta_M + \eta_N)} \qquad (3)$$

where ΔN is the fractional amount of electrons transferred, μ_x is the chemical potential (Mulliken electronegativity) of the respective species, and η_x is the chemical hardness of the

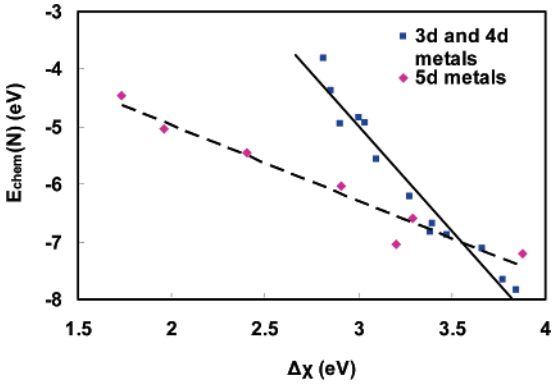

Figure 4. Correlation observed between transition metal and N electronegativity (Mulliken) difference (ΔX) and N−transition metal chemisorption strength. The 3d and 4d metals are seen to fall along the same line with $R^2 = 0.95$. Interestingly, the 5d metals are observed to lie along a line of smaller gradient with $R^2 = 0.94$.

respective species (in the above expression, the subscripts M and N denote metal and nitrogen, respectively). In this work, both η_x and μ_x are approximated by finite differences using the ionization energy (I_x) and electron affinity (A_x) of the respective species[49]

$$\mu_x = -\chi_x = -\frac{1}{2}(I_x + A_x) \quad \eta_x = \frac{1}{2}(I_x - A_x) \qquad (4)$$

where χ_x denotes Mulliken's definition of electronegativity. Figure 3b shows the agreement between the amount of charge transfer (ΔN) as predicted by eq 3 and the actual atomic charge on the adsorbed N atom; as can be seen, the correlation is good with $R^2 = 0.97$.

There is a very interesting corollary of the above finding. Namely, one may expect the trend in N chemisorption energy to follow the trend in electronegativity difference between the metal and the N atom. This is because the charge transferred from the metal to the N atom and thus the degree of ionicity is primarily controlled by the difference in electronegativity. This is exactly what is found, and not only for the 4d metals but for the 3d and 5d metals also. In Figure 4, the chemisorption energy of atomic nitrogen is plotted against the electronegativity difference between N and the respective metal, as estimated by eq 4, for a selection of 3d, 4d, and 5d metals (values are also given in Table 3). It is interesting to note that the 3d and 4d metals fall on the same line, whereas the 5d metals lie along a separate line of smaller gradient. It is noticed that bonding strength increases with increasing electronegativity difference, i.e., the greater the ionic character of the bond, the stronger it is. Indeed, this is in agreement with Figure 3a, where bond strength is seen to increase with increasing atomic charge on N.

Thus, the strength of N chemisorption across a transition series appears to be determined by the electronegativity of the surface metal atoms (as approximated by Mulliken's definition, using atomic ionization energies and electron affinities). Furthermore, as has been discussed above, the magnitude of E_a for N_2 dissociative adsorption decreases with increasing atomic N chemisorption strength. Because of this fact, the activation energy of N_2 on transition metal surfaces will also be controlled by these charge-transfer processes. With increasing charge transfer, the transition states become more stable and the activation energy decreases. Both the sum of the atomic charges on the N atoms at the transition state and E_a for the dissociative adsorption of N_2 on the flat surfaces of the 4d transition metals

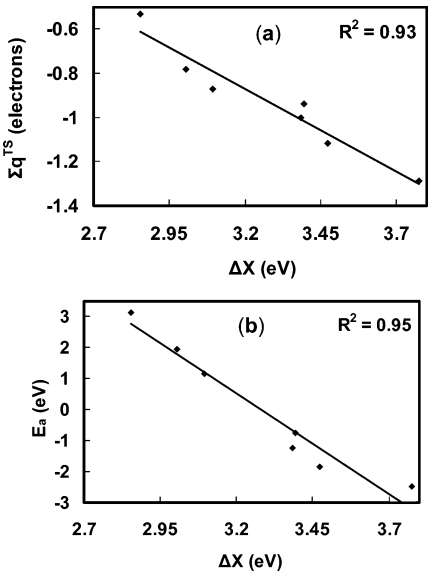

Figure 5. (a) Correlation between the sum of atomic charges on the N atoms at the transition state, as determined by Mulliken charge analysis, and the difference in metal−N electronegativity (ΔX), as estimated by Mulliken's definition using atomic ionization energies and electron affinities. (b) Correlation between the activation energy for the dissociative adsorption of N_2 on the flat surfaces of the 4d transition metals from Zr to Pd and the difference in metal−N electronegativity defined as above.

are plotted against the N-metal electronegativity difference in Figure 5 (Table 1 and Table 3). As can be seen, both the sum of the atomic charges on the N atoms at the transition state and E_a are strongly influenced by the N−metal electronegativity difference.

2. Structure Sensitivity

2.1. Results. In this section, we address structure sensitivity. Specifically, we examine how the activation energy differs between monatomic step sites and flat regions. To achieve this, we have modeled surfaces containing monatomic steps for the same 4d transition metals as considered in the previous section. The dissociation of N_2 has been calculated at these steps, and the corresponding E_a values have been compared to those from the previous terrace calculations. As the dissociation of N_2 has been considered on stepped surfaces across the 4d transition series from Zr to Pd, we have generated stepped surfaces for HCP, BCC, and FCC metals.

Extensive calculations were performed in order to determine the most stable transition state complex formed between N_2 and the step for each metal surface. Slight variations were however observed in how the N atoms bind at the active site on moving across the period. In the case of the early transition metals, the N atom which sits at the step edge also forms bonds with the metal atoms at the base of the step. Figure 6a and b shows the step transition state structures for Zr and Nb, respectively. As can be seen, the step edge N atom at the Zr step is bonding to 4 metal atoms, and actually shares the bonding of two of these with the N atom sitting at the hollow site. In the case of Nb, the step-edge N atom bonds with 3 metal atoms but shares the bonding of none of these with the second metal atom. The Mo transition state is observed to be the same as that of Nb. From Tc through Pd, the step-edge N atom is found to bond with only the two step edge metal atoms and share no bonding of surface metal atoms with the N atom sitting at the hollow site. Figure 6c and d are the transition state geometries observed at Ru and Rh steps, respectively, and illustrate this configuration.

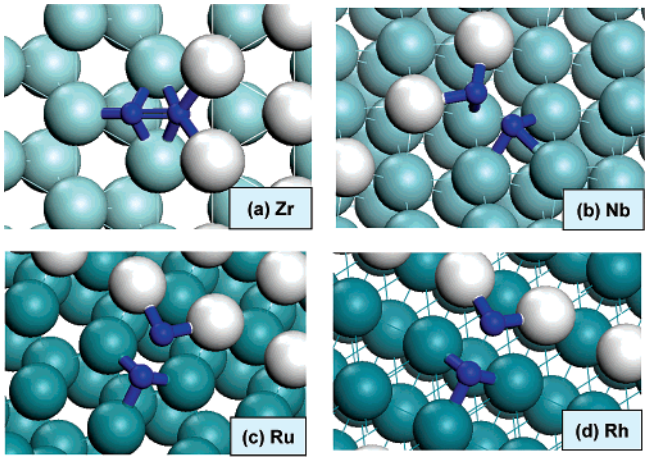

Figure 6. Calculated step-site transition state geometries. (a) Transition state configuration observed at a step site on Zr(001). (b) Transition state geometry observed at steps on Nb(210) and Mo(210). (c and d) Transition state structures determined for a step site on Ru(001) and Rh(211), respectively.

TABLE 4: Main Geometrical Parameters for Our Calculated Step-Site Transition States[a]

surface	d(M−N^{SE}) Å	d(M−N^{T}) Å	d(N−N) Å	E_a(eV)
Zr-stepped	2.281	2.124	1.652	−3.048
Nb(210)	2.086	2.123	1.760	−2.554
Mo(210)	2.087	2.058	1.674	−1.597
Tc-stepped	1.927	1.986	1.788	−1.567
Ru-stepped	1.891	1.972	1.807	−0.509
Rh(211)	1.888	1.969	1.988	0.715
Pd(211)	1.859	1.925	2.422	1.818

[a] d(M−N^{SE}) refers to the average metal−N distance for the step-edge atom, d(M−N^{T}), the average metal−N distance for the N atom sitting at the terrace at the base of the step, and d(N−N), the distance between the N atoms. The activation energies (E_a) correspond to the lowest energy reaction pathways for the dissociative adsorption of N_2 at monatomic steps on the surfaces of the 4d metals from Zr to Pd.

The geometrical parameters for the most stable step transition states are given in Table 4.

Our calculated activation energies for the dissociative adsorption of N_2 at step sites on the surfaces of the 4d transition metals are given in Table 4. These values are also plotted in Figure 2 alongside the activation energies for the reaction occurring on flat regions. We can see immediately from Figure 2 that the activation energy is lower at steps for all of the metals considered in this work. It is also observed that the differences in E_a at the monatomic steps and the flat regions are more marked on the right-hand side of the periodic table. Interestingly, the dissociative adsorption of N_2 shows the lowest structure sensitivity on Mo and the greatest structure sensitivity on Ru. In the next subsection, we provide a detailed analysis of the above observations.

2.2. Analysis and Discussion. We begin our analysis of structure sensitivity by first considering the activation energies for the dissociation of N_2 at step sites. These values have been decomposed in the same manner as those in the previous section for the reaction on terraces. Decomposition values for the reaction occurring at step sites are given in Table 5. The first thing to notice from these data is that for the early transition metals (Zr, Nb, and Mo) the step-edge N atom interacts more strongly with the surface than the N atom on the terrace below the step. Moreover, from Tc onward, with the exception of Ru, the terrace N atom shows the strongest interaction with the surface. In the case of Ru, the chemisorption energy of the step-

TABLE 5: Activation Energy Decomposition Analysis for the Dissociative Adsorption of N_2 at Step Sites (4d metals)[a]

surface	E_{chem}(N*) step edge (eV)	E_{chem}(N*) terrace (eV)	ΣE_{chem}(N*) (eV)	E_{int} (eV)
Zr-stepped	**−7.814**	−6.683	−14.497	1.863
Nb(210)	**−7.138**	−6.524	−13.662	1.521
Mo(210)	**−6.858**	−6.282	−13.140	1.960
Tc-stepped	−5.688	**−6.159**	−11.847	0.693
Ru-stepped	**−5.401**	−5.370	−10.771	0.675
Rh(211)	−4.565	**−4.664**	−9.229	0.358
Pd(211)	−3.711	**−4.209**	−7.920	0.151

[a] E_{chem}(N*) is the individually calculated chemisorption energy of N at the denoted transition state position. ΣE_{chem}(N*) is the sum of the N chemisorption energy at the transition state, and E_{int} is the intramolecular interaction energy between the N atoms at the transition state.

edge N atom and the terrace N atom are seen to be approximately equal.

Both the chemisorption energy of the step-edge N and the N sitting at the terrace below the step decrease on moving across the period from left to right. Thus, ΣE_{chem}(N*) also decreases in this direction. It is worth noticing that, in the case of the early transition metals (Zr, Nb, and Mo), E_{int} is around 1 eV greater than values corresponding to the later metals. This may relate to the fact that, in the case of Zr, Nb, and Mo, the step-edge N atom also forms bonds to terrace atoms at the base of the step (Figure 6a and b). In the case of later metals, however, the step-edge N atoms bond only with the two step edge atoms (Figure 6c and d).

We will now analyze how E_a changes when the reaction occurs at a step site rather than on a flat region (terrace). This is achieved by comparing decomposition data corresponding to each situation. The first thing to consider is how the total chemisorption energy changes (the change in ΣE_{chem}(N*) in going from a terrace transition state to a step site transition state). This is illustrated in the form of a bar chart in Figure 7a; negative values correspond to a decrease in total chemisorption energy. It can be seen that chemisorption energy is lost in the case of Zr and Tc. There is, however, a gain in ΣE_{chem}(N*) for the rest of the of the metals. We now turn our attention to how the repulsive interaction energy changes in going from terrace transition states to step-site transition states. This is again represented in the form of a bar chart in Figure 7b; here, negative values correspond to an increase in repulsive energy (E_{int}). As we can see, there is generally a significant reduction in E_{int} in going from a terrace to a step site, the exceptions being Nb and Mo, where there is an increase in E_{int}.

We are now in a position to explain the salient features of Figure 2, namely, that structure sensitivity is more pronounced on the right-hand side of the periodic table (Ru, Rh, and Pd) and particularly high and low structure sensitivity is observed for Ru and Mo, respectively. As we have seen in Figure 7a, there is generally a favorable electronic effect in going from a terrace to a step site; Zr and Tc are the exceptions. That is, the potential chemisorption energy generally increases. Furthermore, Figure 7b has shown that there is generally a favorable geometric effect when comparing step-site transition states to those on terraces, namely, that the repulsive interaction energy is significantly reduced. The exceptions in this case are Nb and Mo.

We can therefore see that when comparing step-site reactivity to terrace reactivity only in the case of Ru, Rh, and Pd (the late transition metals) do both the electronic and geometric effects contribute to the lowering of the activation energy. The more pronounced structure sensitivity seen in late transition metals

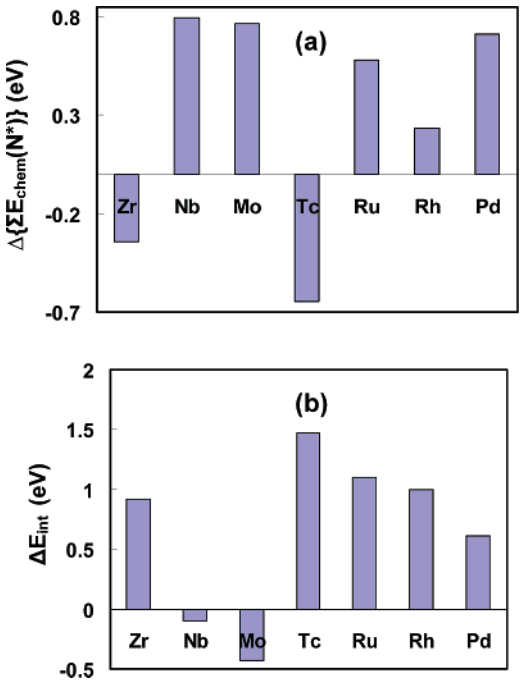

Figure 7. (a) Change in total transition state chemisorption energy (ΣE_{chem}(N*)) in going from a terrace transition state to a step-site transition site (4d metals). Negative values correspond to a loss in chemisorption energy. (b) Change in the intramolecular interaction energy (E_{int}) in going from terrace to step-site transition states. Negative values correspond to a gain in repulsion.

is therefore the result of geometric and electronic effects working in combination. Regarding the early transition metals, the favorable electronic effect for Nb and Mo is reduced by an unfavorable geometric effect. In the same way, the favorable geometric effect observed for Zr and Tc is diminished by an unfavorable electronic effect. That is to say, for the early transition metals, the electronic and geometric effects are seen to work in opposition; this results in only a moderate lowering of activation energy at step sites. Indeed, we can also see why the lowest structure sensitivity is observed for Mo and the highest for Ru. In the case of Mo, there is the largest percentage opposition between electronic and geometric effects, which in turn results in the activation energy being only weakly reduced at the step site, relative to the terrace. Ru on the other hand, represents the largest favorable combination of the two effects, which results in a significant lowering of E_a at the step site relative to the terrace.

Conclusion

The dissociative adsorption of N_2 has been studied over the 4d transition metals using a density functional theory methodology. We have analyzed in detail both trends in reactivity and structure sensitivity. With regards to reactivity, the following points can be made:

(i) We have found that the trend in E_a across the transition series is primarily determined by the total chemisorption energy at the transition state; furthermore, the chemisorption energy at the transition state is found to be almost equal in value to that of the final state, due to the relatively weak interaction between the N atoms at the transition state.

(ii) The trend in chemisorption energy at the final (equilibrium state) state across the period is determined mainly by charge transfer from the surface metal atoms to N, i.e., the ionicity of the metal−N bond.

(iii) The N chemisorption energy trend across the 3d, 4d, and 5d metals can be predicted by the difference in Mulliken electronegativity between N and the metal, as this provides a measure of the ionicity of the metal−N bond.

(iv) Since the trend in E_a follows that of N chemisorption energy, the difference in Mulliken electronegativity between the metal and N provides a good measure of reactivity when comparing metals across a series.

From our analysis of the differences in reactivity between step sites and terraces across the 4d transition series, the following conclusions can be made with respect to structure sensitivity:

(i) The difference in E_a between a step site and a terrace, i.e., structure sensitivity, is greater on the right-hand side of the transition series.

(ii) In going from a terrace to a step active site, both the electronic and geometric effects serve to either lower or raise the activation energy. In the case of the early 4d metals, these effects work in opposition, whereas from Ru onward they work in combination which results in the more marked structure sensitivity observed for the late transition metals.

(iii) The greatest structure sensitivity is observed for Ru, where both the geometric effect and electronic effect significantly reduce E_a at the step site. Mo shows the least structure sensitivity; in this case, the electronic effect and geometric effect show the greatest percentage opposition.

References and Notes

(1) Masel, R. I. *Principles of Adsorption and Reaction on Solid Surfaces*; Wiley: New York, 1996.

(2) Somorjai, G. A. *Introduction to Surface Chemistry and Catalysis*; Wiley: New York, 1994.

(3) Woodruff, D. P.; Delchar, T. A. *Modern Techniques in Surface Science*; Cambridge, 1989.

(4) Aika, K. I.; Tamaru, K. In *Ammonia: Catalysis and Manufacture*; Nielson, A., Ed.; Springer-Verlag: Berlin, 1995.

(5) Ertle, G. *Catal. Rev.—Sci. Eng.* **1980**, *21*, 201.

(6) Tennison, S. R. In *Catalytic Ammonia Synthesis Fundamentals and Practice*; Jennings, J. R., Ed.; Plenum: New York, 1991.

(7) Hagen, S.; Barfod, R.; Fehrmann, R.; Jacobsen, C. J. H.; Teunissen, H. T.; Chorkendoff, Ib. *J. Catal.* **2003**, *214*, 327.

(8) Logadottir, A.; Norskov, J. K. *J. Catal.* **2003**, *220*, 273.

(9) Siporin, S. E.; Davis, R. J.; Rarog-Pilecka, W.; Szmigiel, D.; Kowalczyk, Z. *Catal. Lett.* **2004**, *93*, 61.

(10) Hinrichsen, O.; Rosowski, F.; Hornung, A.; Muhler, M.; Ertle, G. *J. Catal.* **1997**, *165*, 33.

(11) Dietrich, H.; Jacobi, K.; Ertle, G. *J. Chem. Phys.* **1997**, *106*, 9313.

(12) Dahl, S.; Taylor, P. A.; Tornqvist, E.; Chorkendorff, I. *J. Catal.* **1998**, *178*, 679.

(13) Morgan, G. A.; Kim, Y. K.; Yates, J. T. *Surf. Sci.* **2005**, *598*, 1.

(14) Gong, X.-Q.; Ravel, R.; Hu, P. *J. Chem. Phys.* **2005**, *122*, 024711.

(15) Vannice, M. A. *Catal. Rev.—Sci. Eng.* **1976**, *14*, 153.

(16) Schulz, H. *Appl. Catal. A* **1999**, *186*, 3.

(17) Schulz, H.; Claeys, M. *Appl. Catal. A* **1999**, *186*, 91.

(18) Dry, M. E. *Catal. Today* **2002**, *71*, 227.

(19) Davis, B. H. *Fuel Process. Technol.* **2001**, *71*, 157.

(20) Liu, Z.-P.; Hu, P. *J. Am. Chem. Soc.* **2002**, *124*, 11568.

(21) Feibelman, P. J.; Hamann, D. *Phys. Rev. Lett.* **1984**, *52*, 61; *Surf. Sci.* **1985**, *149*, 48.

(22) Falicov, L. M.; Somorjai, G. A. *Proc. Natl. Acad. Sci. U.S.A.* **1985**, *82*, 2207.

(23) Parr, R. G.; Yang, W. *Proc. Natl. Acad. Sci. U.S.A.* **1985**, *82*, 6723.

(24) Harris, J.; Andersson, S. *Phys. Rev. Lett.*. **1985**, *55*, 1583.

(25) Hammer, B.; Norskov, J. K. *Surf. Sci.* **1995**, *343*, 211.

(26) Evans, M. G.; Polanyi, N. P. *Trans. Faraday Soc.* **1936**, *32*, 1333.

(27) Michaelides, A.; Liu, Z.-P.; Zhang, C. J.; Alavi, A.; King, D. A.; Hu, P. *J. Am. Chem. Soc.* **2003**, *125*, 3705.

(28) Logadottir, A.; Rod, T. H.; Norskov, J. K.; Hammer, B.; Dahl, S.; Jacobsen, C. J. H. J. Catal. *J. Catal.* **2001**, *197*, 229.

(29) Jacobsen, C. J.; Dahl, S.; Clausen, B. S.; Bahn, S.; Logadottir, A.; Norskov, J. K. *J. Am. Chem. Soc.* **2001**, *123*, 8404.

(30) Norskov, J. K.; Bligaard, T.; Logadottir, A.; Bahn, S.; Hansen, L. B.; Bollinger, M.; Bengaard, H.; Hammer, B.; Sljivancanin, Z.; Mavrikakis, M.; Xu, Y.; Dahl, S.; Jacobsen, C. J. *J. Catal.* **2002**, *209*, 275.

(31) Hammer, B.; Nielson, O. H.; Norskov, J. K. *Catal. Lett.* **1997**, *46*, 31.

(32) Liu, Z.-P.; Hu, P. *J. Am. Chem. Soc.* **2003**, *125*, 1958.

(33) Dahl, S.; Logadottir, A.; Egeberg, R. C.; Larsen, J. H.; Chorkendorff, I.; Tornqvist, E.; Norskov, J. K. *Phys. Rev. Lett.* **1999**, *83*, 1814.

(34) Hammer, B. *Phys. Rev. Lett.* **1999**, *83*, 3681.

(35) Pearson, R. G. *J. Am. Chem. Soc.* **1963**, *85*, 3533.

(36) Pearson, R. G. *Hard and Soft Acids and Bases*; Dowden, Hutchison and Ross: Stroudsburg, PA, 1973.

(37) Pearson, R. G. *J. Chem. Educ.* **1968**, *45*, 581.

(38) Parr, R. G.; Donnelly, R. A.; Levy, M.; Palke, W. E. *J. Chem. Phys.* **1978**, *68*, 3801.

(39) Payne, M. C.; Teter, M. P.; Allan, D. C.; Arias, T. A.; Joannopoulos, J. D. *Rev. Mod. Phys.* **1992**, *64*, 1045.

(40) Perdew, J. P.; Burke, K.; Ernzerhof, M. *Phys. Rev. Lett.* **1996**, *77*, 3865.

(41) Michaelides, A.; Hu, P. *J. Am. Chem. Soc.* **2000**, *122*, 9866.

(42) Crawford, P.; Hu, P. *J. Chem. Phys.* **2006**, *124*, 044705.

(43) Crawford, P.; Hu, P. *J. Phys. Chem. B.* **2006**, *110*, 4157.

(44) Schwegmann, S.; Seitsonen, A. P.; Dietrich, H.; Bludau, H.; Over, H.; Jacobi, K.; Ertle, G. *Chem. Phys. Lett.* **1997**, *264*, 680.

(45) Cao, Z.; Wan, H.; Zhang, Q. *J. Chem. Phys.* **2003**, *119*, 9178.

(46) Rodriguez, J. A.; Goodman, D. W. *Science* **1992**, *257*, 897.

(47) Segall, M. D.; Shah, R.; Pickard, C. J.; Payne, M. C. *Phys. Rev. B.* **1996**, *54*, 16317.

(48) Parr, R. G.; Pearson, R. G. *J. Am. Chem. Soc.* **1983**, *105*, 7512.

(49) Parr, R. G.; Yang, W. *Density Functional Theory of Atoms and Molecules*; Oxford University Press: Oxford, U.K., 1989.